ChemComm

COMMUNICATION

View Article Online
View Journal | View Issue

Cite this: *Chem. Commun.*, 2025, **61**, 14923

Received 16th July 2025,
Accepted 22nd August 2025

DOI: 10.1039/d5cc04003e

rsc.li/chemcomm

Optimal design of Ru–Sn oxide catalysts for enhanced oxygen evolution reaction using the cluster-plus-glue-atom model

Yue Yu,[ab] Guikai Zhang,[b] Ruqi Wang,[b] Pengfei An,[b] Shengqi Chu,[b] Yue Lu,*[a] Manling Sui [a] and Juncai Dong *[b]

Using the cluster-plus-glue-atom model, we optimized Ru–Sn oxide catalysts for the oxygen evolution reaction (OER). Optimal performance is achieved when all glue-atom sites are occupied by Sn (*i.e.*, Ru : Sn = 1 : 2), thereby maximizing both OER activity and stability. This work provides novel insights and a rapid strategy for designing efficient, stable Ru-based catalysts.

Water electrolysis is vital for sustainable hydrogen production, meeting global energy demands while addressing environmental concerns.[1–3] Proton exchange membrane water electrolysis (PEMWE) stands out for its high current densities, low resistance losses, high hydrogen pressure, and minimal gas crossover.[4,5] However, the acidic environment, high energy barrier, and slow kinetics of the anodic oxygen evolution reaction (OER) process necessitate catalysts with enhanced activity and long-term stability, currently confining options to costly, scarce iridium-based materials. Ruthenium-based catalysts present a compelling alternative, offering superior activity at approximately one-tenth the cost of iridium. Recent advances, beyond interface and stress engineering, have significantly enhanced Ru site activity and catalyst stability through heteroatom doping, forming Ru–O–M (M = Mn, Cr, Er, *etc.*) configurations.[6–8] Nevertheless, the optimal heteroatom concentration and its effect on electrolysis performance remain underexplored, with few theoretical frameworks to guide catalyst design. This study employs the cluster-plus-glue-atom model, originally developed for complex metallic alloys, to clarify the activity origins of Ru–O–Sn configurations and to optimize Sn doping levels based on good structural compatibility between Ru and Sn oxides. Compared with conventional trial-and-error strategies based on experimental experience or density functional theory (DFT) calculations in previous studies of heteroatom-doped Ru-based catalysts (*e.g.*, Mn, Cr, Er), this approach enables direct tracking of the catalyst's chemical short-range order, rapidly identifies optimal compositions, and substantially reduces both experimental workload and computational cost, facilitating the rational design of efficient, cost-effective, and scalable PEMWE systems for hydrogen production.

The cluster-plus-glue-atom model describes material composition and structure as a nearest-neighbor cluster coordinated with a few outer-shell glue-atoms, expressed by the cluster formula [cluster](glue-atoms).[9] According to the principles of atomic density and cluster separation,[10,11] the cluster formula for rutile-structured materials like RuO_2 is [Ru–O_6]Ru_2,[12] where a central Ru atom is coordinated by six O atoms to form the [Ru–O_6] cluster, interconnected by two Ru glue-atoms to create a three-dimensional structure (see Fig. S1 for details). This formula reveals local Ru–O–Ru pairs formed among the center-atom, nearest-neighbor O atoms, and glue-atoms (second-neighbor Ru), driven by chemical short-range order. Our prior studies show that glue-atoms are more readily substituted by heteroatoms.[13,14] While the cluster-plus-glue-atom model has been applied to the design of photocatalysts,[15] it has not yet been utilized for electrocatalyst design. When a heteroatom M replaces glue-atoms, a Ru–O–M local structure forms, with the number of M atoms tied to the glue-atom count. Accordingly, we designed four RuO_2 catalyst samples with varying Sn heteroatom doping levels to study the effect of Sn glue-atom quantities on performance. Specifically, for sample without heteroatom doping, the cluster formula remains [Ru–O_6]Ru_2, denoted as Ru#Ru_2. For partial Sn replacement of glue-atoms, the cluster formula is [Ru–O_6]RuSn, denoted as Ru#RuSn. When glue-atoms are fully replaced by Sn, the cluster formula is [Ru–O_6]Sn_2, denoted as Ru#Sn_2 (see Fig. 1(a)). Finally, when glue-atoms are fully Sn and the center-atom is partially replaced, the formula is [$Ru_{0.5}Sn_{0.5}$–O_6]Sn_2, denoted as $Ru_{0.5}Sn_{0.5}$#Sn_2.

Ru–Sn oxides were synthesized *via* pyrolysis, with the composition of four samples controlled by varying the Ru : Sn ratio

[a] *Beijing Key Laboratory of Microstructure and Property of Advanced Materials, College of Materials Science and Engineering, Beijing University of Technology, Beijing 100124, China. E-mail: luyue@bjut.edu.cn*
[b] *Beijing Synchrotron Radiation Facility, Institute of High Energy Physics, Chinese Academy of Sciences, Beijing 100049, China. E-mail: dongjc@ihep.ac.cn*

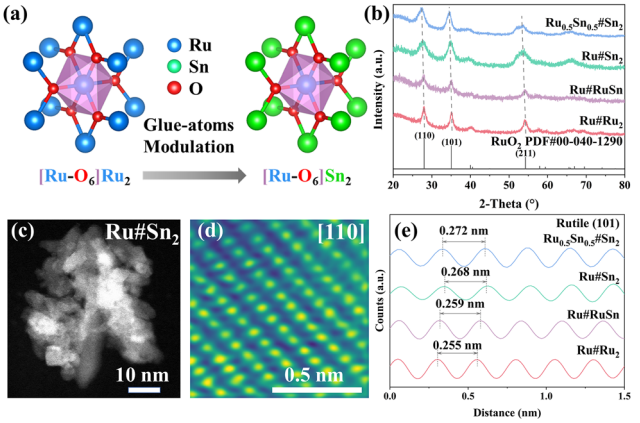

Fig. 1 (a) Schematic illustration of composition design based on cluster-plus-glue-atom model. (b) XRD patterns of Ru–Sn oxides. (c) low and (d) high-magnification HAADF-STEM images of Ru#Sn_2. (e) Scans of the (101) lattice distance of Ru–Sn oxides.

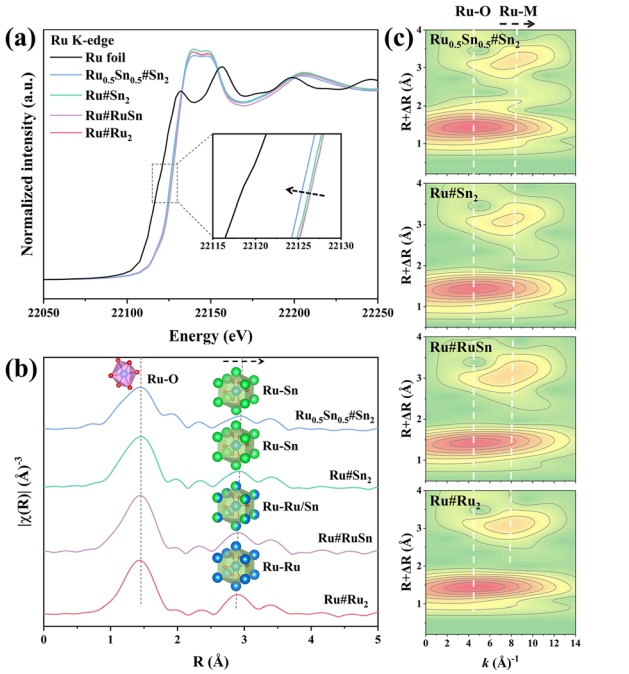

Fig. 2 (a) Ru K-edge XANES spectra, (b) Fourier transform spectra of k^2-weight Ru K-edge EXAFS spectra, (c) Wavelet transforms for the k^2-weighted EXAFS for Ru–Sn oxides.

in the precursor reagents. X-Ray diffraction (XRD) patterns of the four samples all exhibit a single-phase rutile structure that match well with the reference pattern PDF#00-040-1290 (Fig. 1(b)), indicating the formation of a stable Ru–Sn oxide solid solution. Due to the larger ionic radius of Sn (0.69 Å) than Ru (0.62 Å), diffraction peaks shift to lower angles with increasing Sn content.[16] Scanning electron microscopy (SEM, Fig. S2b) and low-magnification HAADF-STEM (Fig. 1(c)) images reveal that Ru#Sn_2 sample consists of uniform granular particles with a size of approximately 10 nm. Fig. 1(d) illustrates the atomic distribution along the [110] crystal orientation, further confirming that Ru#Sn_2 possesses a rutile structure. Similar morphological uniformity is observed across all four samples (Fig. S2–S5), suggesting that varying Ru : Sn ratios have minimal impact on particle morphology, thus reducing surface-related effects on catalytic performance. In addition, high-magnification HAADF-STEM images show the interplanar spacings of rutile facets, such as 0.255 nm for the (101) plane in Ru#Ru_2, 0.275 nm in $Ru_{0.5}Sn_{0.5}$#Sn_2, and 0.334 nm for the (110) plane in Ru#RuSn. As shown in Fig. 1(e), the (101) interplanar spacing increases with the increasing Sn content, further confirming lattice expansion due to the larger Sn cations, consistent with the XRD results. Energy-dispersive spectroscopy (EDS) mapping reveals uniform distribution of Ru and Sn without segregation (Fig. S2–S5), and quantitative analysis (Table S1) confirms that the atomic ratios align with the designed compositions.

X-ray absorption spectroscopy (XAS) was utilized to probe the local electronic structure and coordination environment of Ru–Sn oxides. The Ru K-edge X-ray absorption near-edge structure (XANES) spectroscopies (Fig. 2(a)) for all four samples closely resemble that of pure RuO_2 (Ru#Ru_2), and an increase in Sn content leads to a shift of the absorption edge toward lower energy as compared to pure RuO_2 (Ru#Ru_2), indicating electron accumulation on Ru and a reduced oxidation state due to Sn doping.[8] Meanwhile, the Fourier-transformed extended X-ray absorption fine structure (FT-EXAFS) at the Ru K-edge (Fig. 2(b) and Fig. S6) shows a primary peak at 1.49 Å, which can be attributed to Ru–O scattering, confirming the formation of [Ru–O_x] cluster with oxygen as the first nearest neighbor.[17] In absence of anion doping, oxygen acts as a bridging ligand in the Ru–O–Sn structure. It is noteworthy that the second major peak, resulting from Ru–M (M = Ru/Sn) scattering, shifts from 3.10 Å to 3.15 Å as the Sn content increase, indicating a gradual transition of the glue-atoms from Ru to Sn within the [Ru–O_6] Ru_2 cluster formula of RuO_2. To further investigate the differences in glue-atoms within the molecular-like structural units of RuO_2, a wavelet transform (WT) analysis of the EXAFS spectra was conducted owing to its capability to discriminate the types of coordinating atoms in both *R*-space and *k*-space.[18] As shown in Fig. 2(c), the contour intensity maxima corresponding to the Ru–M scattering increase from 7.93 $Å^{-1}$ for Ru#Ru_2 to 8.03 $Å^{-1}$ for [Ru–O_6]RuSn, 8.17 $Å^{-1}$ for [Ru–O_6]Sn_2, and 8.36 $Å^{-1}$ for [$Ru_{0.5}Sn_{0.5}$–O_6]Sn_2, further corroborating the progressive replacement of Ru glue-atoms with Sn.[19]

The OER activities of Ru#Sn_2, Ru#RuSn, $Ru_{0.5}Sn_{0.5}$#Sn_2 and Ru#Ru_2 were assessed using a three-electrode system in a 0.5 M H_2SO_4 solution. Fig. 3(a) displays the polarization curves obtained through linear sweep voltammetry (LSV), utilizing an electrochemical workstation to normalize the current. At a current density of 10 mA cm^{-2}, the Ru#Sn_2 demonstrates a lower overpotential (η_{10}) of 193 mV compared to Ru#RuSn (226 mV), $Ru_{0.5}Sn_{0.5}$#Sn_2 (237 mV) and Ru#Ru_2 (245 mV). Moreover, the Tafel slope of Ru#Sn_2 in Fig. 3(b) is 49.5 mV dec^{-1}, significantly lower than the other catalysts. The above results indicate that when the same geometric area is coated with the catalyst, Ru#Sn_2 exhibits a lower electrochemical reaction energy barrier and faster reaction kinetics.[20] The

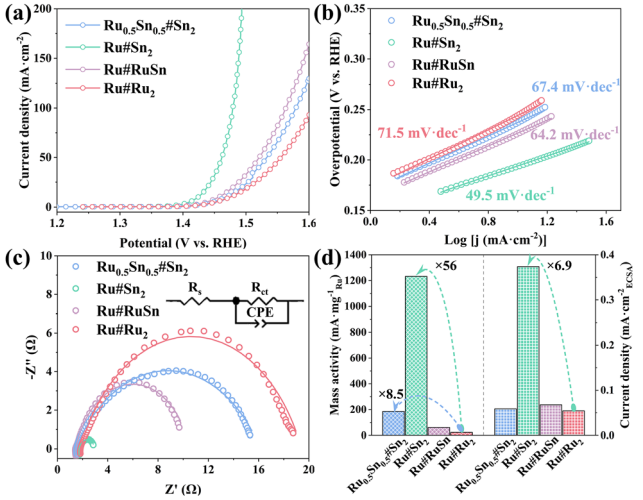

Fig. 3 Electrocatalytic OER performance evaluation for Ru–Sn oxides in 0.5 M H_2SO_4. (a) LSV polarization curves, (b) Tafel plot. (c) Nyquist plots of EIS and fitting result with equivalent circuit. (d) Ru mass activities and ECSA normalized activities of Ru–Sn oxides at potentials of 1.50 V (*vs.* RHE).

electrochemical impedance spectroscopy (EIS) measurements were employed to investigate the charge transfer resistance (R_{ct}) of different catalysts. Based on Fig. 3(c) and the fitting results presented in Table S2, it can be concluded that the R_{ct} of $Ru\#Sn_2$ is 1.28 Ω, the lowest among the four catalysts. This suggests that $Ru\#Sn_2$ exhibits superior electron transfer efficiency during water electrolysis.[21] To investigate the intrinsic activity of the catalytic center, both mass-specific and areal activity were examined and the calculation results are shown in Fig. 3(d). Firstly, the electrochemical double-layer capacitance (C_{dl}) was measured to determine the electrochemically active surface area (ECSA). The results shown in Fig. S7, S8 reveal that $Ru\#Sn_2$ possesses the highest Cdl (30.74 mF cm^{-2}) and the greatest number of active sites, attributable to its larger conductivity and specific surface area. The ECSA-normalized activity at 1.50 V (*vs.* RHE) is 0.37 mA cm^{-2}, indicating that $Ru\#Sn_2$ exhibits the strongest intrinsic OER activity.[22] Furthermore, the mass-specific activities of 4 catalysis are shown at different overpotentials in Fig. S9a, the Ru mass activity of $Ru\#Sn_2$ at 1.50 V (*vs.* RHE) is calculated to be 1232.19 mA mg^{-1}_{Ru}, which is 56 times higher than that of $Ru\#Ru_2$. It is noteworthy that the mass-specific activity of $Ru_{0.5}Sn_{0.5}\#Sn_2$ is 8.5 times higher than that of $Ru\#Ru_2$ at the same potential, demonstrating the enhancing effect of Sn positioned at the glue-atom site on the intrinsic activity of the center Ru sites.[23] On the other hand, the chronopotentiometry (CP) tests (Fig. S9b) shown that $Ru\#Sn_2$ and $Ru_{0.5}Sn_{0.5}\#Sn_2$ can stably react for more than 100 and 40 hours at 10 mA cm^{-2} with a potential growth rate of 0.90 and 2.43 mV h^{-1}, respectively. Ru#RuSn and $Ru\#Ru_2$ can only sustain the reaction for 20 hours. These results suggest that Sn, as a glue-atom, can better maintain the structural stability of the [Ru–O_x] clusters. By comparing descriptors such as η_{10}, Tafel slope, R_{ct}, C_{dl} and CP (Fig. S10), it can be concluded that $Ru\#Sn_2$ with all glue-atoms occupied by Sn exhibits the strongest intrinsic activity at the center Ru site. Although $Ru_{0.5}Sn_{0.5}\#Sn_2$ also has all glue-atoms as Sn, part of its center-atoms is substituted with Sn and showing no significant catalytic activity. In cases where there are fewer Sn glue-atoms of $Ru\#Sn_2$ and $Ru\#Ru_2$, the modification over the Ru center is insufficient, resulting in poor catalytic performance.

The OER mechanism and stability of Ru–Sn oxides were investigated using DFT calculations, focusing on the (110) facet of the rutile structure due to its high activity.[24,25] Bader charge analysis (Fig. 4(a)) reveals electron transfer from Sn to Ru, decreasing the Ru charge transfer from 1.83 ($Ru\#Ru_2$) to 1.68 ($Ru\#Sn_2$), consistent with XAS results. The differential charge density reveals electron accumulation on glue-atoms and the central Ru in $Ru\#Ru_2$, whereas in $Ru\#Sn_2$, electrons concentrate more on the Ru center with less on Sn glue-atoms (isosurface level: 0.015), thereby indicating an enhanced regulation of the catalytic Ru center by Sn glue-atoms. Fig. 4(b) shows the partial and total density of states (PDOS and TDOS). The d-band center of Ru 4d in $Ru\#Sn_2$ exhibits a notable upshift to −1.41 eV, closer to the Fermi level compared to that of $Ru\#Ru_2$ (−1.64 eV). This observation indicates optimized adsorption of oxygenated intermediates and faster OER kinetics.[26] Furthermore, the TDOS results (Fig. S11) indicate that $Ru\#Sn_2$ exhibits more density of states near the Fermi level, suggesting improved conductivity and charge transfer.[27] Gibbs free energy was calculated to investigate the thermodynamic energy barrier for OER. As shown Fig. 4(c), it reveals that $Ru\#Sn_2$ has a lower energy barrier (1.88 eV) for the rate-determining step (*OH → *O + H^+ + e^-) compared to $Ru\#Ru_2$ (2.11 eV), balancing intermediate adsorption better than $Ru\#Ru_2$, which strongly adsorbs *O, hindering further *OH adsorption. On the other hand, to understand the difference in stability between $Ru\#Sn_2$ and $Ru\#Ru_2$, the formation energy of Ru vacancy (Ru_v) and the projected crystal orbital Hamilton population (pCOHP) were

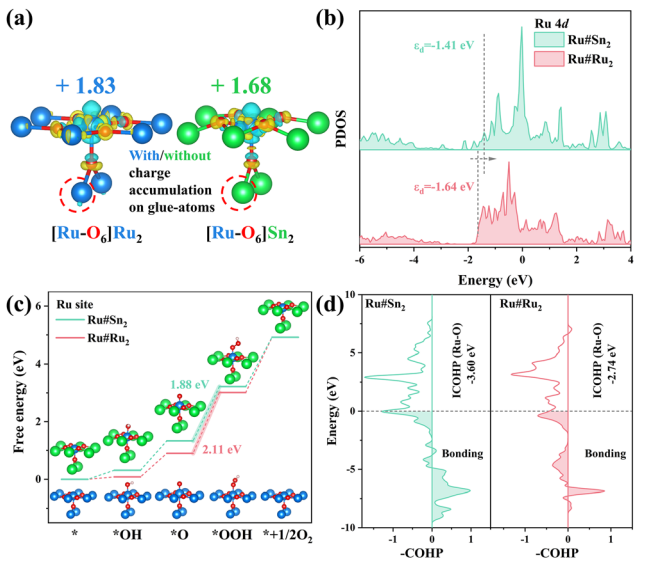

Fig. 4 (a) Differential charge density and Bader charge calculation of $Ru\#Ru_2$ and $Ru\#Sn_2$. (b) The PDOS of Ru 4d for $Ru\#Ru_2$ and $Ru\#Sn_2$. (c) Gibbs free energy diagrams on Ru site at U = 0 V for $Ru\#Ru_2$ and $Ru\#Sn_2$. (d) COHP of $Ru\#Sn_2$ and $Ru\#Ru_2$.

calculated. Fig. S12 shows a higher Ru demetallization energy barrier in Ru#Sn_2 (1.18 eV) compared to Ru#Ru_2 (−0.79 eV), indicating greater resistance to Ru dissolution. pCOHP analysis (Fig. 4(d)) shown that Ru#Sn_2 has more bonding states below the Fermi level compared to Ru#Ru_2, resulting in a smaller integrated COHP (ICOHP) value of −3.60 eV for Ru#Sn_2 *versus* −2.74 eV for Ru#Ru_2. This indicates a stronger Ru–O bonding interaction in Ru#Sn_2, resulting in enhanced structural stability during OER.[28]

In conclusion, we synthesized Ru–Sn oxide catalysts with varying center and glue-atom compositions using the cluster-plus-glue-atom model. Experimental and theoretical analyses demonstrate that optimal OER activity and stability are achieved when all glue-atoms are Sn (Ru : Sn = 1 : 2), maximizing regulation of the Ru center-atom. Insufficient Sn glue-atoms (RuO_2 or Ru : Sn = 2 : 1) reduce catalytic center optimization, while fewer Ru center-atoms (Ru : Sn = 1 : 5) decrease active site density, lowering activity. This study offers novel insights and a rapid design approach for high-performance ruthenium-based OER catalysts.

This work was financially supported by the National Key Research and Development Program of China (2021YFA1502200), the Youth Innovation Promotion Association of the Chinese Academy of Sciences (Y2022006), the Innovation project of the Institute of High Energy Physics of Chinese Academy of Sciences, the National Natural Science Foundation of China (12422401), and the Excellent Youth Fund of Beijing Natural Science Foundation (JQ24009). The authors would like to thank the BL17B1 beamline of Shanghai Synchrotron Radiation Facility for XAS measurements.

Conflicts of interest

There are no conflicts to declare.

Data availability

The data supporting this article have been included as part of the SI. See DOI: **https://doi.org/10.1039/d5cc04003e**

Notes and references

1 Y. Jiao, Y. Zheng, M. Jaroniec and S. Z. Qiao, *Chem. Soc. Rev.*, 2015, **44**, 2060–2086.
2 B. Liu, J. Dong, H. Wang, J. Chen, S. Liu, X. Xiong, Y. Yuan and X. Zeng, *Chem. Commun.*, 2025, **61**, 2357–2360.
3 L. Gao, X. Cui, Z. Wang, C. D. Sewell, Z. Li, S. Liang, M. Zhang, J. Li, Y. Hu and Z. Lin, *Proc. Natl. Acad. Sci. U. S. A.*, 2021, **118**, e2023421118.
4 R.-T. Liu, Z.-L. Xu, F.-M. Li, F.-Y. Chen, J.-Y. Yu, Y. Yan, Y. Chen and B. Y. Xia, *Chem. Soc. Rev.*, 2023, **52**, 5652–5683.
5 F. Wang, X. Gong, Y. Cao and J. Tan, *Chem. Eng. Sci.*, 2025, **311**, 121601.
6 M. Qi, X. Du, X. Shi, S. Wang, B. Lu, J. Chen, S. Mao, H. Zhang and Y. Wang, *J. Am. Chem. Soc.*, 2025, **147**, 18295–18306.
7 Y. Shen, X.-L. Zhang, M.-R. Qu, J. Ma, S. Zhu, Y.-L. Min, M.-R. Gao and S.-H. Yu, *Nat. Commun.*, 2024, **15**, 7861.
8 L. Li, G. Zhang, C. Zhou, F. Lv, Y. Tan, Y. Han, H. Luo, D. Wang, Y. Liu, C. Shang, L. Zeng, Q. Huang, R. Zeng, N. Ye, M. Luo and S. Guo, *Nat. Commun.*, 2024, **15**, 4974.
9 C. Dong, Q. Wang, J. B. Qiang, Y. M. Wang, N. Jiang, G. Han, Y. H. Li, J. Wu and J. H. Xia, *J. Phys. D: Appl. Phys.*, 2007, **40**, R273.
10 J. Chen, Q. Wang, Y. Wang, J. Qiang and C. Dong, *Philos. Mag. Lett.*, 2010, **90**, 683–688.
11 D. Dong, S. Zhang, Z. Wang, C. Dong and P. Häussler, *Mater. Des.*, 2016, **96**, 115–121.
12 Y. Ma, D. Dong, A. Wu and C. Dong, *lnorg. Chem.*, 2018, **57**, 710–717.
13 Y. Yu, S. Zhang, S. Liu, Y. Ren, Z. Xia, N. Wang, H. Wang, W. Jiang, C. Liu, W. Ding, Z. Zhang and C. Dong, *J. Alloys Compd.*, 2022, **926**, 166771.
14 Y. Yu, S. Liu, H. Wang, S. Zhang, N. Wang, W. Jiang, C. Liu, W. Ding, Z. Zhang and C. Dong, *Vacuum*, 2022, **203**, 111315.
15 Y. Yu, S. Liu, H. Wang, S. Zhang, N. Wang, W. Jiang, C. Liu, W. Ding, Z. Zhang and C. Dong, *J. Solid State Chem.*, 2023, **317**, 123694.
16 Y. Xu, Z. Mao, J. Zhang, J. Ji, Y. Zou, M. Dong, B. Fu, M. Hu, K. Zhang, Z. Chen, S. Chen, H. Yin, P. Liu and H. Zhao, *Angew. Chem., Int. Ed.*, 2024, **63**, e202316029.
17 Z.-Y. Wu, F.-Y. Chen, B. Li, S.-W. Yu, Y. Z. Finfrock, D. M. Meira, Q.-Q. Yan, P. Zhu, M.-X. Chen, T.-W. Song, Z. Yin, H.-W. Liang, S. Zhang, G. Wang and H. Wang, *Nat. Mater.*, 2023, **22**, 100–108.
18 S. Zhao, C. Tan, C.-T. He, P. An, F. Xie, S. Jiang, Y. Zhu, K.-H. Wu, B. Zhang, H. Li, J. Zhang, Y. Chen, S. Liu, J. Dong and Z. Tang, *Nat. Energy*, 2020, **5**, 881–890.
19 Q. Ji, B. Tang, X. Zhang, C. Wang, H. Tan, J. Zhao, R. Liu, M. Sun, H. Liu, C. Jiang, J. Zeng, X. Cai and W. Yan, *Nat. Commun.*, 2024, **15**, 8089.
20 L. Wu, F. Zhang, S. Song, M. Ning, Q. Zhu, J. Zhou, G. Gao, Z. Chen, Q. Zhou, X. Xing, T. Tong, Y. Yao, J. Bao, L. Yu, S. Chen and Z. Ren, *Adv. Mater.*, 2022, **34**, 2201774.
21 G. Zhang, J. Pei, Y. Wang, G. Wang, Y. Wang, W. Liu, J. Xu, P. An, H. Huang, L. Zheng, S. Chu, J. Dong and J. Zhang, *Angew. Chem., Int. Ed.*, 2024, **63**, e202407509.
22 Z. Dong, C. Zhou, W. Chen, F. Lin, H. Luo, Z. Sun, Q. Huang, R. Zeng, Y. Tan, Z. Xiao, H. Huang, K. Wang, M. Luo, F. Lv and S. Guo, *Adv. Funct. Mater.*, 2024, **34**, 2400809.
23 H. Jin, S. Choi, G. J. Bang, T. Kwon, H. S. Kim, S. J. Lee, Y. Hong, D. W. Lee, H. S. Park, H. Baik, Y. Jung, S. J. Yoo and K. Lee, *Energy Environ. Sci.*, 2022, **15**, 1119–1130.
24 R. R. Rao, M. J. Kolb, L. Giordano, A. F. Pedersen, Y. Katayama, J. Hwang, A. Mehta, H. You, J. R. Lunger, H. Zhou, N. B. Halck, T. Vegge, I. Chorkendorff, I. E. L. Stephens and Y. Shao-Horn, *Nat. Catal.*, 2020, **3**, 516–525.
25 R. R. Rao, M. J. Kolb, N. B. Halck, A. F. Pedersen, A. Mehta, H. You, K. A. Stoerzinger, Z. Feng, H. A. Hansen, H. Zhou, L. Giordano, J. Rossmeisl, T. Vegge, I. Chorkendorff, I. E. L. Stephens and Y. Shao-Horn, *Energy Environ. Sci.*, 2017, **10**, 2626–2637.
26 C. Wang, X. Wu, H. Sun, Z. Xu, C. Xu, X. Wang, M. Li, Y. Wang, Y. Tang, J. Jiang, K. Sun and G. Fu, *Energy Environ. Sci.*, 2025, **18**, 4276–4287.
27 S. Liu, Z. Zhang, K. Dastafkan, Y. Shen, C. Zhao and M. Wang, *Nat. Commun.*, 2025, **16**, 773.
28 C. Zhou, L. Li, Z. Dong, F. Lv, H. Guo, K. Wang, M. Li, Z. Qian, N. Ye, Z. Lin, M. Luo and S. Guo, *Nat. Commun.*, 2024, **15**, 9774.

